Research Article

Dominik Banat*

Load-carrying capacity of the GFRP and CFRP composite beams subjected to three-point bending test – numerical investigations

https://doi.org/10.2478/mme-2019-0037
Received Jun 7, 2018; revised Sep 10, 2018; accepted Nov 20, 2018

Abstract: The subject of this article is the finite element method (FEM) simulation of the multi-layered rectangular composite beam subjected to three-point bending test. The study is focused on the composite beams made of glass or carbon fibre-reinforced laminates (glass fibre-reinforced polymer [GFRP] and carbon fibre-reinforced polymer [CFRP]) for which different laminate stacking were addressed. Three beam geometries with various length-to-thickness ratios included short beam shear (SBS) test, provided the beam is short relative to its thickness, which maximised the induced shear stresses. Simulation included the application of Tsai–Hill, Hoffman, Tsai–Wu, Hashin and Puck failure criteria to perform the composite beam failure analysis wherein the matrix and fibre failure were considered separately. Numerical failure studies also aimed to verify the beam failure modes and the participation of stress tensor elements in material failure.

Keywords: FEA, composite material, FRP, failure criteria, flexural test

1 Introduction

Composite structures are one of the most commonly used structural materials that have been increasingly used in the recent years with significant developments in the aviation, automotive, wind power, sport equipment and transport industries. This is due to the growing demand for lightweight and high-strength materials in order to meet the stringent requirements of modern industry. In fact, however, the rapid development and the use of composite structures began truly after the production of synthetic resins whose adhesion properties are the basis for the production of modern multi-layered laminates [1]. The binding polymer allowed one to produce the fibre-reinforced polymers (FRPs) that are constructed using various laminates that most commonly include either glass fibres (glass fibre-reinforced polymers – GFRP) or carbon fibres (carbon fibre-reinforced polymers – CFRP). Some of the FRP applications, particularly in aviation industry, are based on the unidirectional glass fibre-reinforced prepregs combined with aluminium alloy sheets (Glare type) [2]. Such plies when combined with composite provides high bearing strength, huge impact resistance and improved damage tolerance [3]. Fibre-reinforced material also guarantees improved strength and stiffness, especially when compared to other structural materials on a unit weight basis [3]. More importantly, depending on the fibre orientation in FRP, the structure could be stiffer in one particular direction, which gives an advantage for its industrial applications [4]. Therefore, such laminates are widely used as advanced structural materials in almost all branches of industry, particularly in aviation industry [5, 6]. This has inspired researchers and scientists over the years to investigate the mechanical performance of composites under specific loading conditions [7–9].

One of the key properties concerning the performance of composite structures is the high flexural strength and stiffness, which leads to some kind of a strength-optimising analysis [10]. In fact, the flexural loading applied to a specimen simultaneously induces the tensile, compressive and shear stresses. Therefore, depending on the material strength properties, the initiation of the material failure is imposed by one of these stresses reaching its limiting value or by their combined effect [11]. In addition, in flexure tests, the change in particular stresses along the length of the structure and the stress concentrations is usually observed at the loading and supporting pins [12]. For that reason, the failure criteria (FC) need to be implemented to simultaneously assess the bending and shear performance of the structural element and to take the combined effect of all induced stresses into ac-

***Corresponding Author: Dominik Banat:** Department of Strength of Materials, Lodz University of Technology Stefanowskiego 1/15, 90-924 Lodz, Poland; Email: dominikbanat@gmail.com

count [13]. Herein, as long as isotropic materials are concerned, various FC that can be used to effectively determine the yield point of a material, for example, Huber–Mises–Hencky (HMH) criterion, are available [14]. The issue of appropriate failure criterion is much more complicated for non-isotropic composite materials, where the yield behaviour of the material shows directional dependency [15]. Therefore, strength analysis of the FRP requires the application of the so-called quadratic failure criteria, wherein specific failure factors are determined to allow a direct failure assessment [16]. Particularly for considered composite laminates, the advanced concepts and developments of failure analysis need to be investigated [17].

According to the World-Wide Failure Exercise (WWFE), till date, there is no particularly satisfying method in the finite element method (FEM) to analyse the propagation of the multi-failure modes in the composite material [18, 19]. In the literature, one can find various examples of numerical failure analysis for thin-walled composite columns subjected to compression tests [20–22]. However, there are relatively few studies devoted to the analysis of failure mechanisms of composite structures subjected to flexural tests [23, 24]. Therefore, an attempt to investigate damage mechanics and its impact on the structure stability for flexural tests needs to be taken. The purpose of this study is to reveal the FEM results of failure analysis performed for GFRP and CFRP beams subjected to three-point bending test.

2 Subject of the study

2.1 Three-point bending test

Comprehensive numerical study of three-point bending test was conducted to take into account various material responses in different beam types. The analysis included short beam shear (SBS) test method that subjected a beam to bending, provided the beam is short relative to its thickness. The objective was to maximise the induced shear stress because it is presumed that for a beam with a ratio of $l/h = 4–5$, the shear effect dominates the material response. On the other hand, the ratio $l/h = 32$ induces higher flexural (tensile and compressive) stresses, whereas for ratio $l/h = 10–12$, both shear and bending stresses contribute significantly to beam failure. Therefore, in the following study, different beam geometries were assumed to analyse all three cases of three-point flexure test and to simultaneously assess the shear (V) and bending (M) performances of the proposed composite beams (see Figure 1). From the shear force and bending moment diagrams, it is clear that there is a stress concentration at the point where force is applied.

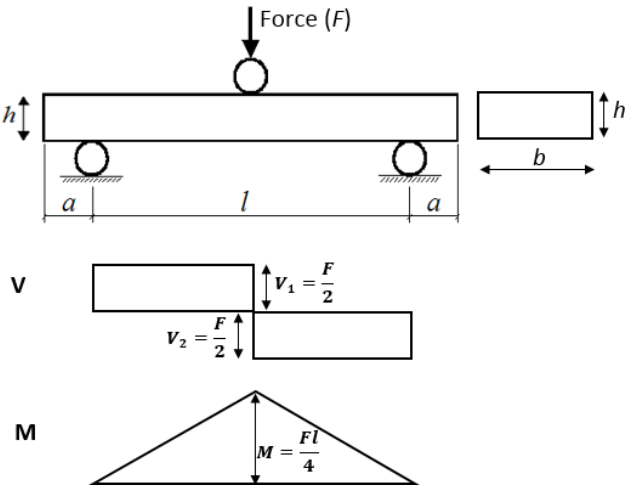

Figure 1: Three-point bending scheme with given support span-to-thickness ratio (l/h)

Three different beam types (I, II and III) with various span length-to-specimen thickness ratios (l/h) of 4, 12 and 32, respectively, were considered. The height and width of the beam were assumed to be constant, that is, $h = 4$ mm and $b = 20$ mm. The thickness of single lamina present in the eight-layered composite was 0.5 mm. The distance between the support pins and the beam ends (denoted as a) was assumed to be approximately 20% of the support span length (Table 1).

Table 1: Various beam types depending on l/h ratio

Beam type	Support span length, l (mm)	Distance, a (mm)	Height, h (mm)	Width, b (mm)
I, $l/h = 4$	16	3.5	4	20
II $l/h = 12$	48	10	4	20
III $l/h = 32$	128	26	4	20

2.2 Fibre-reinforced polymer

Comparative analysis was carried out for two different fibre-reinforced laminates that concerned glass fibres (GFRP) or carbon fibres (CFRP). The laminate stacking consisted of 8 layers, and depending on fibres orienta-

tions, two different lay-ups combinations were developed: $[0_8]_T$ and $[90_8]_T$. In addition, for comparison reasons, some results were also presented for the laminate stacking $[(45/-45)_4]_T$ and $[(0/90)_4]_T$. Elastic properties and the strength limits of applied generic E-glass-epoxy and carbon-epoxy composites were adopted from the literature [25] and summarised in Table 2. For the FRP composite analysis, the material properties were determined according to specific rules [26] in the main orthotropic directions that coincide with fibre orientation (principal 1 axis).

Table 2: Mechanical characteristics of the GFRP and CFRP composites

Mechanical properties	GFRP	CFRP
Longitudinal tensile modulus, E_1 (GPa)	39	140
Transverse tensile modulus, E_2 (GPa)	8.6	11
Shear modulus, G_{12} (GPa)	3.8	5.5
Poisson's ratio, ν_{12}	0.28	0.27
Longitudinal tensile strength, X_t (MPa)	1080	2000
Longitudinal compressive strength, X_c (MPa)	620	1200
Transverse tensile strength, Y_t/Z_t (MPa)	39	50
Transverse compressive strength, Y_c/Z_c (MPa)	128	170
Shear strength, S (MPa)	89	70

The implementation of such stress limits in the direction longitudinal and transverse to the orientations of the fibres allows one to effectively apply the failure criteria. In addition, the Puck failure criterion requires specifying the inclination parameters that need to be determined for FRPs according to specific guidelines given separately for GFRP and CFRP [27].

3 Numerical modelling procedures

Numerical analysis was performed using a commercial software package ANSYS®. Using SOLID185, the eight-layered composite beam was initially generated with each layer defined as the separate volume. In addition, three elements were defined along the layer thickness to take into account the bending effect in further analysis. Consequently, the VGLUE option was used to redefine the layered volumes along their intersections that merged areas, lines and key points at the common boundary volumes. Finally, homogeneous structural solid of eight-layered composite beam was created (Figure 2a). In addition, local coordinate systems were defined in the separate volumes that formed the basis for orthotropic material principal directions in each element (see Figure 2b).

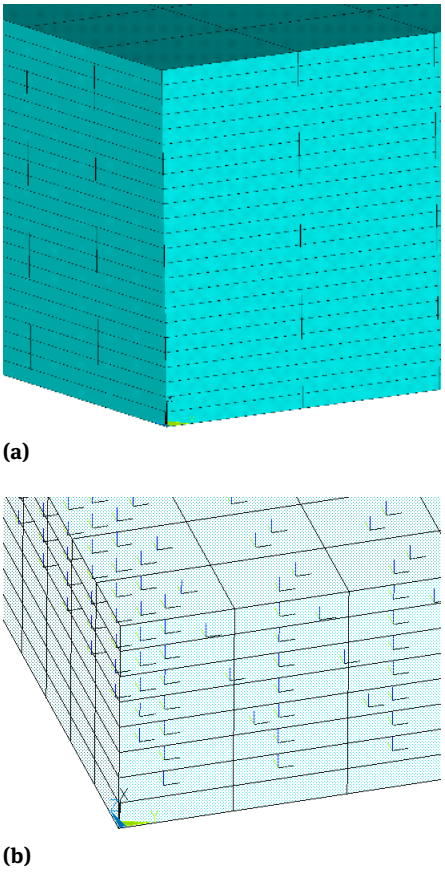

Figure 2: Structural solid of (a) eight-layered composite beam and (b) element coordinate systems referenced to material orthotropic axes

Various beam geometries were modelled based on different support span-to-thickness ratios (l/h). For that reason, the support span length (l) and the distance between the support pins and the beam ends (a) were variable, whereas the width (b) and height/thickness (h) of the beam were constant for each considered beam type (Figure 3). Consequently, three various beam geometries were distinguished for the determined support span-to-thickness ratios (l/h) – see Table 1.

Boundary conditions (BC) in each variant were similarly defined in the form of simply supported constraints that blocked appropriate kinematic degrees of freedom for both the beam edges. On one side of the beam, the pinned support was assumed, whereas on the other side, the roller support was assumed. For that reason, nodes located at the pinned support were fully constrained in

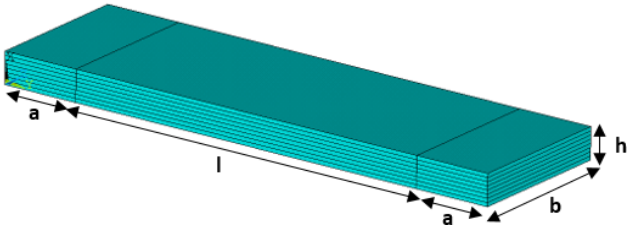

(a)

Figure 3: Dimensions of the beam geometry

translations, whereas nodes at the roller support were permitted to translate in only one direction along the surface on which the roller rests. Depending on the beam type, the displacement constraints were applied along the beam length to simulate the position of supporting pins. Arbitrarily beam type II (l/h = 12) was chosen to reveal the assumed BC in Figure 4. In FE model, the bending was realised by applying the concentrated load at the beam middle span. Herein, load was applied perpendicular to the layer plane. Specific nodes along the beam mid-span were also coupled (ux = const) to guarantee that they will take the same displacement in the axial direction when subjected to external load. This allowed for minimising the effect of stress concentration at the node where the load was applied. The BCs defined in this manner simulated the simply supported beam subjected to three-point bending test.

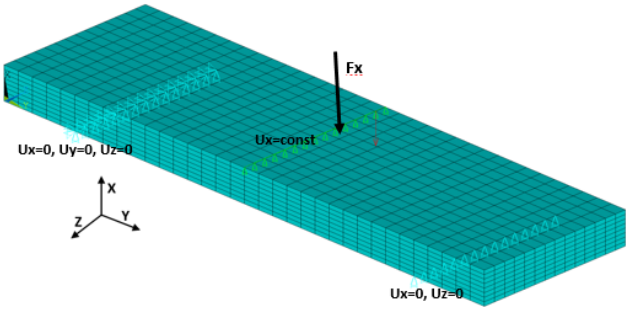

Figure 4: Beam design with corresponding boundary conditions

4 FEM computations

Numerical methods were initially introduced to analyse the deflection in the middle of the beam. This allowed one to verify the FE model and its corresponding BCs for three-point bending test. Analysis was carried out simultaneously for two element type models, that is, SOLID185 and SHELL181. First, a linear-static analysis was conducted to determine the nodal solution of deformed mode shape for each beam design. Subsequently, a nonlinear analysis was conducted, which included the large deflection effect to account for the geometric nonlinearities. The nonlinear problem was solved by the incremental Newton–Raphson procedure whereby the stiffness matrix was updated with each iteration. To avoid convergence difficulties, the arc-length method was also activated. Finally, equilibrium paths were estimated for composite beams of GFRP and CFRP material type. Beam response to three-point flexure test was investigated in full load range. Equilibrium paths available for FEA SOLID185 and SHELL181 element types were compared. This allowed one to verify the implemented element types, modelling procedures and to confirm the applied BCs.

Numerical calculations included an attempt to estimate the potential damage of the beam subjected to three-point bending test. The strength analysis of the GFRP and CFRP beams was conducted either at each single layer separately or at the entire laminate treated as the homogeneous structure. For such fibre-reinforced laminates, various failure criteria were considered to indicate the failure initiation. Those that were finally chosen for the purpose of this study are the Tsai–Hill, Hoffman, Tsai–Wu, Hashin and Puck failure criteria, which are most commonly applied to investigate FRP [18]. Herein, the failure assessment required the implementation of the Tsai–Hill and Hoffman failure criteria, which are not readily available in Ansys application. Therefore, it was crucial to use the advanced user-programmable features (UPFs) that allowed one to write the Fortran routines for non-available failure criteria [28]. The so-called user-written failure criteria were defined as the macro codes that were run straightforward from the Ansys Mechanical APDL interface. Finally, the failure criteria were introduced to nonlinear analysis with the incremental load in order to observe the change in failure factors in each load step. Subsequently, the results were mapped onto the profile geometry that allowed one to distinguish the position greatly exposed to damage. Further analysis was conducted to assess the participation of the stress tensor elements in the beam failure.

5 Results and discussion

5.1 Beam deflection

At the initial stage, FEA of the three-point bending test estimated the deformed mode shapes of the beam geome-

try subjected to flexural loading. Structural displacements were displayed for three different beam types (I, II and III) in the direction coincident with the loading plane. The results are presented for the material GFRP with fibre alignment $[0_8]_T$ in Figure 5. Such analysis indicated considerably different deformed mode shapes depending on the beam geometry. Beams of higher support span-to-thickness ratios (l/h = 12, l/h = 32) provided significantly higher middle-span deflection than the short beam (l/h = 4).

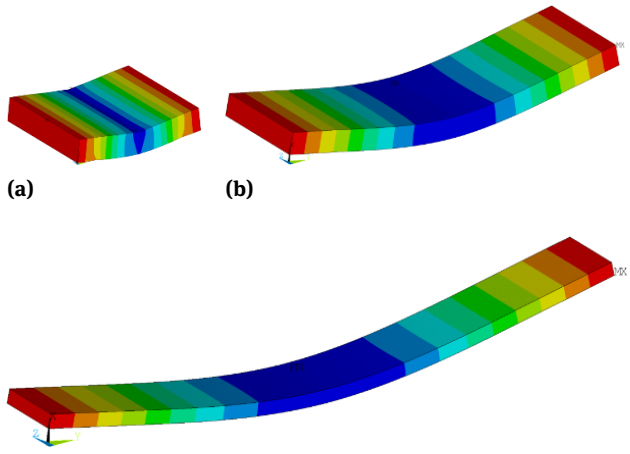

Figure 5: Deformed modes for GFRP [08]T beam types: (a) I (l/h = 4), (b) II (l/h = 12) and (c) III (l/h = 32)

Subsequently, the nonlinear analysis was conducted to estimate the equilibrium paths for three-point flexure test. The equilibrium paths allowed one to estimate the relationship between the loads applied to the beam structure as a function of middle span deflection. Comparative analysis for GFRP material in three beam types (l/h = 4, l/h = 12 and l/h = 32) is presented in Figure 6. Different fibre orientations in the legend were marked in the following manner: [1]a–$[0_8]_T$, [2]a–$[90_8]_T$, [3]a–$[(45/\text{-}45)_4]_T$, [4]a–$[(0/90)_4]_T$.

For each considered beam types in various laminate configurations, consistent results were obtained within predicted equilibrium paths. The lay-up $[0_8]_T$ was found to be the stiffest for each beam type ratios; however, the stacking $[90_8]_T$ was the most deflected at the beam middle span for the corresponding load. The laminate $[(0/90)_4]_T$ was also stiffer than $[(45/-45)_4]_T$ lay-up. Such analysis for various ply-sequences confirms the biggest advantage of FRP composites that can be designed to have the highest strength in a specific direction depending on the industrial

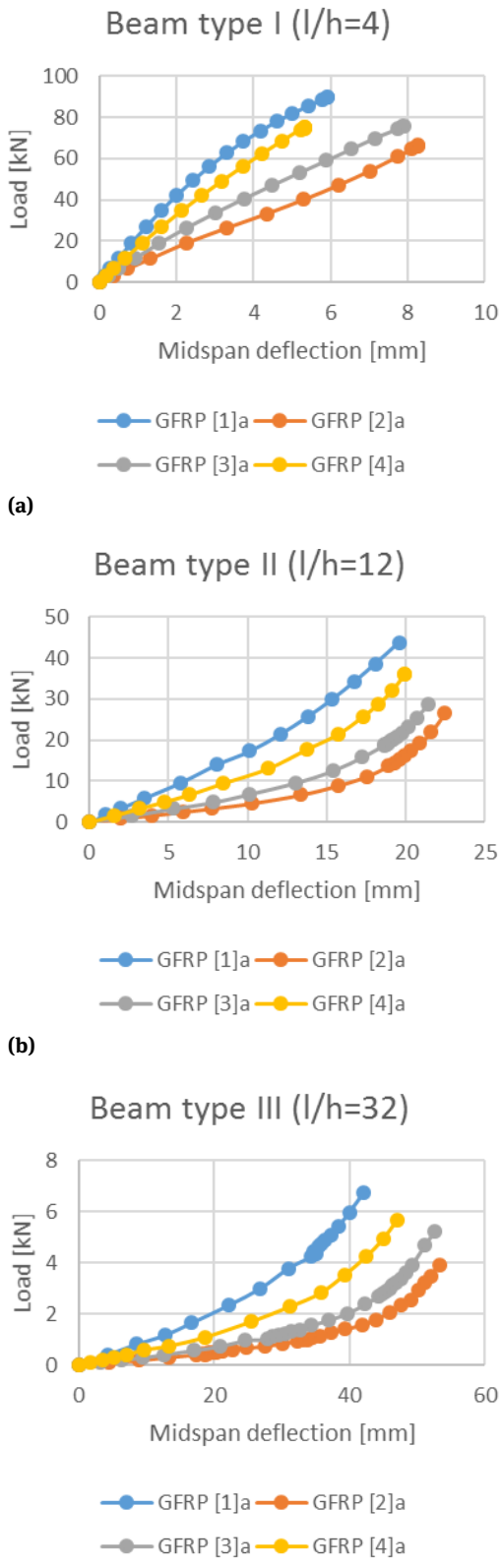

Figure 6: Equilibrium paths for GFRP beam types: (a) I (l/h = 4), (b) II (l/h = 12) and (c) III (l/h = 32)

application. Therefore, presented comparative FE analysis of beam deflection for various beam geometries can give important insights for composite manufacturers.

Importantly, in order to judge the above FEM results obtained for SOLID185 element type, the equilibrium paths were also predicted for numerical model made of SHELL181 element. As an example, the results for GFRP beam types I and III (l/h = 4 and l/h = 32) for two laminate configurations ([1]–$[0_8]_T$, [2]–$[90_8]_T$) are presented in Figure 7. It can be noticed that for beam type III, the FE computations estimate equilibrium paths in the same manner for both finite elements. However, analysis of equilibrium paths in full load range performed for the beam type I indicates that SHELL element type is significantly stiffer than SOLID type. It is due to the inter-laminar normal stresses (INS), which according to software guidelines is not commonly available in shell element formulations [28]. Nevertheless, an attempt should also be taken to perform the corresponding experimental tests to assess unambiguously obtained results and to validate element types implemented in FEA.

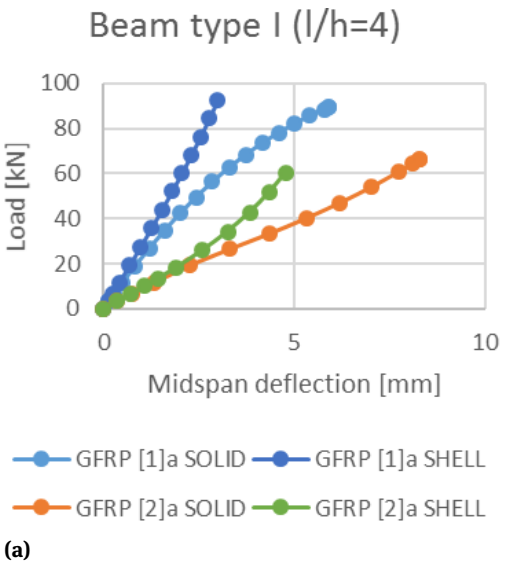

Figure 7: SOLID and SHELL equilibrium paths comparison for beam types (a) I (l/h = 4) and (b) III (l/h = 32)

5.2 Failure assessment

5.2.1 Damaged mode shapes

The structural nonlinear analysis also allowed to analyse the beam-damaged mode shapes. For that reason, the nodal results were determined for the last converged load step solution taken from the estimated equilibrium paths. Estimated in such manner, highest deformations were further mapped onto the beam geometry. The results for short CFRP beam (l/h = 4) are presented in Figure 8. As it can be shown, the damaged modes differ significantly for four considered lay-up configuration of the laminate ($[0_8]_T$, $[90_8]_T$, $[(45/-45)_4]_T$ and $[(0/90)_4]_T$), which corresponded to the predicted equilibrium paths. Similarly, the laminates $[(0)_8]_T$ and $[(0/90)_4]_T$ (Figure 8a, d) are stiffer than the laminates $[90_8]_T$ and $[(45/-45)_4]_T$ (Figure 8b, c) for the considered loading conditions. On the basis of such comparison of the FEM results, different beam geometries can be recommended depending on its industrial application.

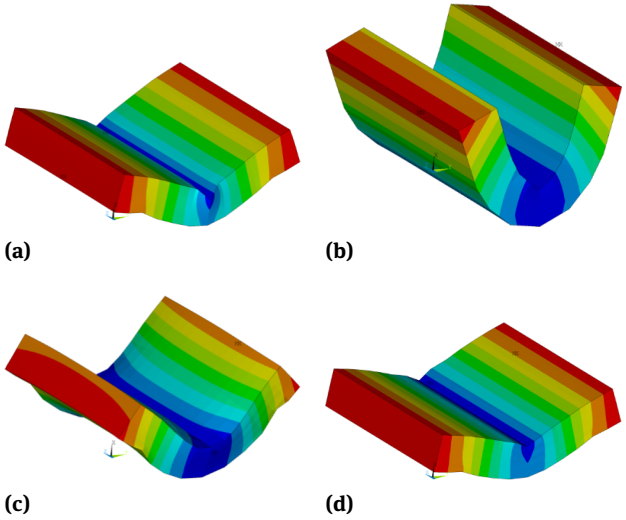

Figure 8: Damaged beam modes of various CFRP composites: (a) [08]T, (b) [908]T, (c) [(45/-45)4]T and (d) [(0/90)4]T

5.2.2 Failure criteria analysis

The failure criteria were applied simultaneously with the structural nonlinear analysis to assess the failure initiation. The strength analysis was conducted for five failure criteria: Tsai–Hill, Hoffman, Tsai–Wu, Hashin, and Puck. Herein, the Hashin and Puck criteria were distinguished for matrix and fibre failure analysis separately. On the basis of that, seven different failure factors were determined: HILL, Tsai–Hill failure criterion; HOFFM, Hoffman failure criterion; TWSR, inverse of Tsai–Wu strength ratio index; HFIB, Hashin fibre failure criterion; HMAT, Hashin matrix failure criterion; PFIB, Puck fibre failure criterion; PMAT, Puck inter-fibre (matrix) failure criterion.

To observe the beam failure performance, failure criteria were analysed for GFRP beam type I ($l/h = 4$) with relation to the load incremental rise. The results of FC analysis determined in this manner for GFRP beam are presented in Figure 9. Such nonlinear analysis shows that first failure initiation (FF > 1) is predicted by quadratic failure criteria (Tsai–Hill, Hoffman and Tsai–Wu). The Hashin and Puck criteria estimate lower FF, wherein in both the cases, the matrix failure is expected before the fibre damage. Various assessment was provided for the Puck criterion, which took into account the inclination parameters that were specified in FEA separately for GFRP and CFRP in accordance to given guidelines [27]. Owing to the high stress concentration, significant difference in failure factors values were noticed for earliest and most simplified Tsai–Hill criterion (HILL), and, therefore, authors do not recommend this criterion for failure analysis of multilayered composite beam subjected to three-point bending test. In each case, failure initiation was caused by stress concentrations observed in the supporting and loading pins. Nevertheless, failure factors obtained by the Hashin (HFIB) and Puck fibre (PFIB) criteria are significantly lower. Low values of both these failure indexes confirm a high strength of unidirectionally reinforced composite beam in the axial direction parallel to fibres.

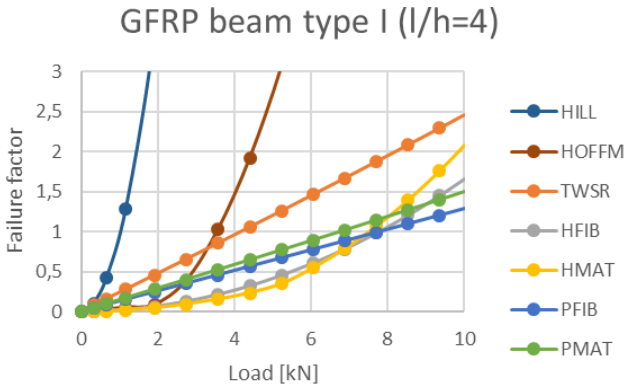

Figure 9: FF for incremental load increase in short GFRP beam ($l/h = 4$) with lay-up [08]T

The results of failure criteria strength analysis were mapped onto the beam profile geometry to indicate particular areas greatly exposed to failure. Maps of FF for each considered criterion were determined in Figure 10. Such failure assessment confirms that fracture occurs along beam middle span where the highest stress concentration is provided by loading pins. FF maximum is also mapped close to the beam mid-plane where in case of short beam test the highest shear stresses are expected. All failure factors exhibit similar damage patterns and failure initiation modes which suggests a good compliance of failure criteria implementation in FE computations.

5.2.3 Participation of stress tensor in material failure

Subsequently, the impact of the stress tensor components on the failure factor values was analysed in separate laminate plies that corresponded to *x, y, z* coordinate system. For that purpose, for each criterion, nodal data were sorted to indicate the maximum FF defined at the current location. For selected in that manner node location, the stress tensor elements were written into data file and gathered in Table 3. Herein, the Hashin criterion was taken into consideration, as there is, in general, an increasing adoption of this criterion especially for the purpose of the failure assessment of the FRP [29].

Such comparative table shows the highest tensile stress σ_x in the bottom layer (L1), the highest compressive stress in the top layer (L8) and high values of shear stresses induced within the middle L5 layer. As it can also be noticed, the greatest values of stress components were not associated with the highest FF for specific nodal data. Differences in failure factors for considered criteria were greatly dependent on the manner how the stress tensor elements were implemented in the failure function. Hence, another analysis was performed to distinguish the stress tensor element that mostly influences the failure factor. Therefore, to verify the results from numerical computations, analytical formulas were also applied for the Hashin fibre, f_f, and the Hashin matrix, f_m, failure criteria (Eqs. 1 and 2).

$$f_f = \begin{cases} \left(\frac{\sigma_x}{X_t}\right)^2 + \frac{{\sigma_{xy}}^2 + {\sigma_{xz}}^2}{{S_{xy}}^2} \; if \; \sigma_x > 0 \\ \left(\frac{\sigma_x}{X_t}\right)^2 if \; \sigma_x < 0 \end{cases} \tag{1}$$

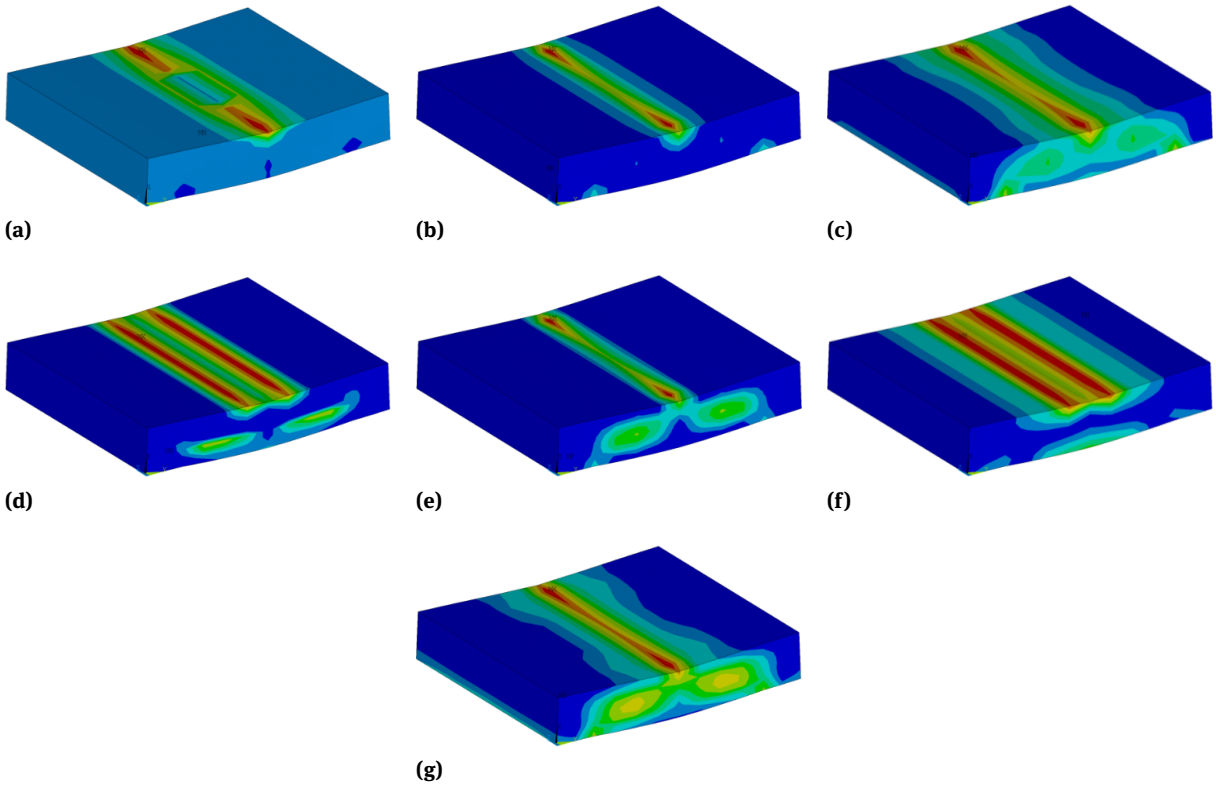

Figure 10: Maps of FF for (a) HILL, (b) HOFFM, (c) TWSR, (d) HFIB, (e) HMAT, (f) PFIB and (g) PMAT

Table 3: Stress tensor elements in beam layers L1, L5 and L8

Layer	Criteria	FF	σ_x	σ_y	σ_z	σ_{xy}	σ_{yz}	σ_{xz}
L1	HFIB	**0.42**	696.68	5.75	−13.33	0.14	2.88	0.00
L1	HMAT	**1.58**	526.81	51.62	−2.87	0.00	0.00	0.01
L5	HFIB	**0.31**	35.12	5.31	−39.14	−0.38	2.74	49.31
L5	HMAT	**1.24**	−101.95	0.92	7.99	3.16	−3.73	96.99
L8	HFIB	**1.66**	−799.36	−66.61	19.11	2.11	0.34	−20.63
L8	HMAT	**2.08**	−485.22	45.88	−255.27	−0.09	8.54	−0.02

$$f_m = \begin{cases} \left(\frac{\sigma_y+\sigma_z}{Y_t}\right)^2 + \frac{{\sigma_{yz}}^2-\sigma_y\sigma_z}{{S_{yz}}^2} + \frac{{\sigma_{xy}}^2+{\sigma_{xz}}^2}{{S_{xy}}^2} \; if\; \sigma_y+\sigma_z > 0 \\ \frac{1}{Y_c}\left[\left(\frac{Y_c}{2S_{yz}}\right)^2 - 1\right](\sigma_y+\sigma_z) + \left(\frac{\sigma_y+\sigma_z}{2S_{yz}}\right)^2 \\ + \frac{\sigma_{yz}^2-\sigma_y\sigma_z}{S_{yz}^2} + \frac{\sigma_{xy}^2+\sigma_{xz}^2}{S_{xy}^2} if\; \sigma_y+\sigma_z < 0 \end{cases} \tag{2}$$

For transversely isotropic model, the allowable stresses for glass-epoxy composite were adopted according to the strength characteristics given in Table 2. Material strengths and substitution of particular stresses into failure criteria functions allowed one to assess the contribution of particular parts to the material failure. In case of the Hashin fibre criterion (HFIB), two formulas were taken into consideration depending on the σ_x sign. Therefore, for $\sigma_x > 0$ in layers L1 and L5, the participation of stress elements was analysed in Table 4, and for $\sigma_x < 0$, it was analysed in Table 5. In the case of Hashin fibre criterion, the analysis imposed that the part of the criterion failure function, including normal stresses σ_x, has the greatest impact on the failure factor in outer layers (L1 and L8), whereas the interaction of shear stresses (σ_{xy}, σ_{xz}) results in the fibre failure in the layer (L5) close to the mid-plane of the beam.

In a similar manner, the Hashin matrix criterion (HMAT) was examined by splitting the failure function formula into specific parts. Note that formula (2) for $\sigma_y + \sigma_z > 0$ is considered in layers L1 and L5 (Table 6) and $\sigma_y + \sigma_z < 0$ is considered in the layer L8 (Table 7). Similarly, the re-

Table 4: Participation of stress tensor elements in the Hashin fibre criterion (f_f) for $\sigma_x > 0$

Layer	$\left(\frac{\sigma_x}{X_t}\right)^2$	$\frac{\sigma_{xy}{}^2+\sigma_{xz}{}^2}{S_{xy}{}^2}$	Sum = HFIB (f_f)
L1	0.42	0.00	**0.42**
L5	0.00	0.31	**0.31**

Table 5: Participation of stress tensor elements in the Hashin fibre criterion (f_f) for $\sigma_x < 0$

Layer	$\left(\frac{\sigma_x}{X_t}\right)^2$	Sum = HFIB (f_f)
L8	1.66	**1.66**

Table 6: Participation of stress tensor elements in the Hashin matrix criterion (f_m) for $\sigma_y + \sigma_z > 0$

Layer	$\left(\frac{\sigma_y+\sigma_z}{Y_t}\right)^2$	$\frac{\sigma_{yz}{}^2-\sigma_y\sigma_z}{S_{yz}{}^2}$	$\frac{\sigma_{xy}{}^2+\sigma_{xz}{}^2}{S_{xy}{}^2}$	Sum = HMAT (f_m)
L1	1.56	0.02	0.00	**1.58**
L5	0.05	0.00	1.19	**1.24**

Table 7: Participation of stress tensor elements in the Hashin matrix criterion (f_m) for $\sigma_y + \sigma_z < 0$

Layer	$\left[\left(\frac{Y_c}{2S_{yz}}\right)^2 - 1\right]\frac{(\sigma_y+\sigma_z)}{Y_c}$	$\left(\frac{\sigma_y+\sigma_z}{2S_{yz}}\right)^2$
L8	−0.79	1.38

$\frac{\sigma_{yz}^2-\sigma_y\sigma_z}{S_{yz}^2}$	$\frac{\sigma_{xy}^2+\sigma_{xz}^2}{S_{xy}^2}$	Sum = HMAT (f_m)
1.49	0.00	**2.08**

sults indicate that the normal stresses dominate the failure in outer layers, whilst the interaction of shear stresses results in matrix failure in layer closer to the beam middle plane. Particularly, the compressive stress, σ_y, contributes mainly to the matrix failure in layers L1 and L8 and the interaction of shear stresses $\sigma_{xy}{}^2 + \sigma_{xz}{}^2$ results in failure in the layer L5. However, there is no possibility of an unambiguous assessment of the type and nature of such matrix failure. Literature data argue that the most common form of matrix failure initiation is rupture on the verge of fibre–matrix joint, which leads to further cracks within specific fibres [30]. Failure in a composite material occurring on the boundary surface of the layer can also provide the interlaminar delamination.

6 Conclusions

This article draws together the results from the FE simulation of the composite beam subjected to three-point bending test. Comparative analysis was performed for GFRP and GFRP. The geometrically nonlinear analysis allowed one to estimate the equilibrium path for various beam types and laminate configuration. Predicted flexural performance was found to be a strong function of ply-stacking sequence, which confirms the laminated beam theory for general three-point bending concept [12]. Herein, FE simulation was found to be in agreement for two element type models, that is, SOLID185 and SHELL181 numerical models. Such results assessment and model verification approved the FEM model for further strength analysis.

Failure assessment allowed to estimate the potential failure initiation of the beam subjected to three-point bending test. For the purpose of this study, Tsai-Hill, Hoffman, Tsai-Wu, Hashin and Puck failure criteria were defined and implemented in FE code. Tsai-Hill and Hoffman criteria were not readily available in the FEM software, and, therefore, according to the literature survey, these were further implemented in FEA using UPFs. Failure factors were finally determined based on stress distributions adopted from particular load step of nonlinear loading process. The results of strength analysis simulation performed for GFRP and CFRP composites allowed to assess the failure initiation either at each single layer separately or at the entire laminate treated as the homogeneous structure. Mapping FF onto the profile geometry indicated regions greatly exposed to damage. Furthermore, the participation of stress tensor components in beam matrix and fibre failure was taken into account and discussed. It was proven for SBS test ($l/h = 4$) that there is a plane of highest shear stresses at or near the mid-plane along the length of the beam. This is where the beam typically fails according to the beam shear test theory. Nevertheless, because of relative short support span length, the stress state along the beam profile was found to be highly affected by the local forces at the loading and supporting pins, which provided high stress concentration that initiated damages.

As it was also shown, the results of considered failure criteria differ mutually and they are greatly dependent on the context of use, that is, laminate material properties and the particular layer position. Therefore, the specific loading condition once predicted as a failure might be considered another way whilst taking different criteria into consideration. Hence, so far, we do not have at our disposal particular satisfactory FC for anisotropic material, and there exist only approximate failure theories that need

to be judged against experimental evidences. Therefore, FEA of three-point test method needs to be judged by experimental evidences in order to validate the obtained results and to give the recommendations for its application.

Acknowledgement: This study was supported by the Ministry of Science and Higher Education of Poland – Diamond Grant No 0037/DIA/2017/46.

I would like to thank my supervisors Professors Zbigniew Kolakowski and Radosław Mania who provided insight and expertise that greatly assisted my research.

References

[1] Jones R.M.: Mechanics of Composite Materials. 2nd ed., Taylor & Francis, Philadelphia, 1999.
[2] Moreira P.M.G.P, Silva L.F.M., Castro P.M.S.T.: Structural connections for lightweight metallic structures. Springer, Berlin, 2012.
[3] Vlot A, Gunnink J.W.: Fibre Metal Laminates: An Introduction, Springer, Dordrecht, 2001.
[4] Czapski P., Kubiak T.: Influence of Fibre Arrangement on the Buckling Load of Composite Plates - Analytical Solution. Fibres and Textiles in Eastern Europe, 5, 92–97, 2015.
[5] Vogelesang L.B., Vlot A.: Development of fibre metal laminates for advanced aerospace structures. Journal of Materials Processing Technology, 103, 1–5, 2000.
[6] Wu G., Yang J.M.: The mechanical behavior of GLARE laminates for aircraft structures. The Journal of the Minerals, Metals & Materials Society, 57, 72–79, 2005.
[7] Mania R.J, York C.B.: Buckling strength improvements for Fibre Metal Laminates using thin-ply tailoring. Composite Structures, 159, 424–432, 2017.
[8] Soltani P., Keikhosravy M., Oskouei R.H. and Soutis C.: Studying the tensile behaviour of GLARE laminates: A finite element modelling approach. Applied Composite Materials, 18, 271–282, 2011.
[9] Banat D., Kolakowski Z. and Mania R.J.: Investigations of FML profile buckling and post-buckling behaviour under axial compression. Thin-Walled Structures, 107, 335-344, 2016.
[10] Valarinho L., Correia J.R. and Branco F.A.: Experimental study on the flexural behaviour of multi-span transparent glass–GFRP composite beams. Construction and Building Materials, 49, 1041–1053, 2013.
[11] Sauvage J.B., Aufray M., Jeandrau J.P., Chalandon P., Poquillon D. and Nardin M.: Using the 3-point bending method to study failure initiation in epoxide-aluminum joints. International Journal of Adhesion and Adhesives, 75, 181–189, 2017.
[12] ASTM D790-03.: Standard Test Method for Flexural Properties of Unreinforced and Reinforced Plastics and Electrical Insulation Materials. ASTM International, 1–11, 2003.
[13] Jakubczak P., Gliszczyński A., Bieniaś J., Majerski K. and Kubiak T.: Collapse of channel section composite profile subjected to bending Part II: Failure analysis. Composite Structures, 179, 1–20, 2017.
[14] Hencky H.: Zur Theorieplastischer Deformationen und der hierdurchim Material hervorgerufenen Nachspannungen. ZeitschriftFür Angewandte Mathematik Und Mechanik, 4, 323–334, 1924.
[15] Banat D. and Mania R.J.: Comparison of failure criteria application for FML column buckling strength analysis. Composite Structures, 140, 806–815, 2016.
[16] Banat D. and Mania R.J.: Failure assessment of thin-walled FML profiles during buckling and postbuckling response. Composites Part B: Engineering, 112, 278–289, 2017.
[17] Altenbach H., Sadowski T.: Failure and Damage Analysis of Advanced Materials. Springer, Udine, 2014.
[18] Kaddour A.S., Hinton M.J., Smith P.A. and Li S.: The background to the third world-wide failure exercise. Journal of Composite Materials, 47, 2417–2426, 2013.
[19] Banat D. and Mania R.J.: Progressive failure analysis of thin-walled Fibre Metal Laminate columns subjected to axial compression. Thin-Walled Structures, 122, 52–63, 2018.
[20] Gliszczynski A. and Kubiak T.: Progressive failure analysis of thin-walled composite columns subjected to uniaxial compression. Composite Structures, 169, 52-61, 2016.
[21] Falkowicz K., Mazurek P., Różyło P., Wysmulski P. and Smagowski W.: Experimental and numerical analysis of the compression thin-walled composite plate. Advances in Science and Technology, 10, 177–184, 2016.
[22] Wysmulski P., Dębski H., Różyło P., Falkowicz K.: A study of stability and post-critical behaviour of thin-walled composite profiles under compression. Eksploatacjai Niezawodnosc - Maintenance and Reliability, 18, 632–637, 2016.
[23] Gliszczyński A. and Kubiak T.: Load-carrying capacity of thin-walled composite beams subjected to pure bending. Thin-Walled Structures, 115, 76–85, 2017.
[24] Urbaniak M., Świniarski J., Czapski P. and Kubiak T.: Experimental investigations of thin-walled GFRP beams subjected to pure bending. Thin-Walled Structures, 107, 397–404, 2016.
[25] Hebda M.: Zastosowanie energetycznego kryterium wytężeniowego do analizy wytrzymałościowej kompozytów włóknistych, Ph. D. Thesis, Cracow University of Technology, 2006.
[26] Barbero E.J.: Finite Element Analysis of Composite Materials. 2nd ed. CRC Press, Boca Raton, 2007.
[27] Puck A., Kopp J. and Knops M.: Guidelines for the determination of the parameters in Puck's action plane strength criterion. Composites Science and Technology, 62, 371–378, 2002.
[28] User's Guide ANSYS® Academic Research, Help System, USA, 2017.
[29] Barbero E.J., Cosso F.A., Roman R. and Weadon T.L.: Determination of material parameters for Abaqus progressive damage analysis of E-glass epoxy laminates. Composites Part B: Engineering, 46, 211–220, 2013.
[30] Dębski H.: Badania numeryczne i doświadczalne stateczności i nośności kompozytowych słupów cienkościennych poddanych ściskaniu. Zeszyty Naukowe. Rozprawy Naukowe, Wydawnictwo Politechniki Łódzkiej,2013.